Int J Earth Sci (Geol Rundsch) (2010) 99:1187–1197
DOI 10.1007/s00531-009-0474-9

ORIGINAL PAPER

Age constraints on faulting and fault reactivation: a multi-chronological approach

Wolfgang Siebel · Horst P. Hann · Martin Danišík · Cosmas K. Shang · Christoph Berthold · Johann Rohrmüller · Klaus Wemmer · Noreen J. Evans

Received: 4 September 2008 / Accepted: 12 July 2009 / Published online: 7 August 2009

Abstract Movement within the Earth's upper crust is commonly accommodated by faults or shear zones, ranging in scale from micro-displacements to regional tectonic lineaments. Since faults are active on different time scales and can be repeatedly reactivated, their displacement chronology is difficult to reconstruct. This study represents a multi-geochronological approach to unravel the evolution of an intracontinental fault zone locality along the Danube Fault, central Europe. At the investigated fault locality, ancient motion has produced a cataclastic deformation zone in which the cataclastic material was subjected to hydrothermal alteration and K-feldspar was almost completely replaced by illite and other phyllosilicates. Five different geochronological techniques (zircon Pb-evaporation, K–Ar and Rb–Sr illite, apatite fission track and fluorite (U-Th)/He) have been applied to explore the temporal fault activity. The upper time limit for initiation of faulting is constrained by the crystallization age of the primary rock type (known as "Kristallgranit") at 325 ± 7 Ma, whereas the K–Ar and Rb–Sr ages of two illite fractions <2 μm (266–255 Ma) are interpreted to date fluid infiltration events during the final stage of the cataclastic deformation period. During this time, the "Kristallgranit" was already at or near the Earth's surface as indicated by the sedimentary record and thermal modelling results of apatite fission track data. (U–Th)/He thermochronology of two single fluorite grains from a fluorite–quartz vein within the fault zone yield Cretaceous ages that clearly postdate their Late-Variscan mineralization age. We propose that later reactivation of the fault caused loss of helium in the fluorites. This assertion is supported by geological evidence, i.e. offsets of Jurassic and Cretaceous sediments along the fault and apatite fission track thermal modelling results are consistent with the prevalence of elevated temperatures (50–80°C) in the fault zone during the Cretaceous.

Keywords Argillic alteration · Fault zone · K–Ar illite · Apatite fission track · (U–Th)/He thermochronology

W. Siebel (✉) · H. P. Hann · M. Danišík · C. K. Shang · C. Berthold
Institut für Geowissenschaften,
Wilhelmstraße 56, 72074 Tübingen, Germany
e-mail: wolfgang.siebel@uni-tuebingen.de

M. Danišík · N. J. Evans
John de Laeter Centre of Mass Spectrometry,
Curtin University of Technology, Perth, WA, Australia

J. Rohrmüller
Bayerisches Landesamt für Umwelt,
Leopoldstr. 30, 95615 Marktredwitz, Germany

K. Wemmer
Geowissenschaftliches Zentrum der Universität Göttingen,
Goldschmidtstrasse 3, 37077 Göttingen, Germany

N. J. Evans
CSIRO Exploration and Mining, ARRC,
26 Dick Perry Avenue, 6151 Perth, WA, Australia

Introduction

Active faults or paleoearthquakes can be dated either by cosmogenic isotopes (see, e.g. Ritz et al. 1995; Fenton et al. 2001), electron spin resonance (e.g. Ikeya et al. 1982), thermoluminescence (e.g. Banerjee et al. 1999), or disequilibrium dating (e.g. Eyal et al. 1992). For ancient fault zones (i.e. those older than several million years) such methods are no longer suitable, and quantitative time constraints are more difficult to achieve. Pseudotachylite layers within ancient fault zones have been successfully

dated by fission track (Murakami and Tagami 2004) and Ar/Ar methods (e.g. Kohút and Sherlock 2003). Ages of older fracture zones can also be obtained using conventional radiometric dating methods if these zones are associated with synkinematic rocks or minerals (e.g. Siebel et al. 2005a, b) or hydrothermal mineralization (e.g. Parry et al. 2001). Notwithstanding these results, unravelling the geological record of fault movement remains challenging because subsequent tectonic processes can lead to partial (or total) replacement of primary minerals and/or resetting of isotopic systems to a variable extent. To date, only a few studies have constrained the time interval between fault formation and reactivation using geochronological methods. For instance, Ar–Ar muscovite dating on mylonites and pseudotachylites from the Møre-Trøndelag Fault, Norway, has revealed that brittle deformation post-dated mylonitization by c. 100 Ma (Sherlock et al. 2004).

Radiometric age constraints on fault zone activity are only reliable if the dated material was completely re-equilibrated isotopically or was newly formed during the deformation process. One mineral that has been utilized as a geochronometer in faults is illite which normally forms as an authigenic clay mineral during burial of pelitic sediments. Illite has been used to date diagenetic processes (e.g. Zhao et al. 1997; Zwingmann et al. 1999), but since this mineral can also be formed during argillic alteration, it provides a means to directly date the formation of fault-related clay gouges (Lyons and Snellenburg 1971; Kralik et al. 1987; Parry et al. 2001; Ylagan et al. 2002; Zwingmann et al. 2004; Solum et al. 2005).

In order to tackle the evolution of faults and to allow for discrimination between the time of formation and later reactivation phases, a multi-chronological approach is warranted. This work studies samples from a section of the Danube Fault where granite has undergone strong clastic deformation. During this process, which was associated with hydrothermal fluorite–quartz mineralization, abundant phyllosilicates, including illite, were formed. We applied five different chronometric dating techniques (zircon Pb-evaporation, K–Ar and Rb–Sr illite, apatite fission track and fluorite (U–Th)/He) on minerals formed during primary magmatic, secondary alteration and hydrothermal processes. Our approach allows the temporal evolution of a given fracture zone locality to be revealed.

Geological background

The Variscan orogen in central Europe resulted from the Late Palaeozoic collision and amalgamation of Laurentia-Baltica, Gondwana, and intervening basement fragments (see, e.g. Ziegler and Dézes (2006)). During final consolidation of this orogen, the Variscan crust was disrupted and dissected into large blocks by numerous crustal-scale fault zones or lineaments (Fig. 1a). Within the Bohemian Massif, a major intraplate system of NW–SE and NE–SW trending faults developed in response to reorganization of tectonic style and stress transfer between Western Europe and the East European platform (Mattern 2001). The Danube Fault together with its sister fault, the Bavarian Pfahl with its well-known quartz-lode (e.g. Peucker-Ehrenbrink and Behr 1993), are impressive examples of NW–SE trending shear zones in the southwestern Bohemian Massif (Fig. 1a). For both faults a dextral sense of displacement has been inferred from shear sense indicators and other structural observations (for more details on fault kinematics see Mattern (1995)).

Although the Danube Fault is one of the most prominent strike-slip faults in central Europe, its age and evolution are poorly constrained and geochronological data have only been obtained in the Austrian section of the fault zone (Brandmayr et al. 1995, see discussion below). The fault runs roughly parallel to the Danube River and nominally extends ~200 km from Regensburg, Germany, to Linz in Austria, where it disappears beneath the Alpine foreland molasse. For about half its distance, it forms the boundary between the uplifted Bohemian Massif and the Mesozoic (Jurassic and Cretaceous) and Miocene sediments which were deposited in nearshore epicontinental seas and in the Alpine foreland basin, respectively. Between Deggendorf and Linz (Fig. 1a) the fault largely cuts through Variscan basement rocks. The contact between the basement and sedimentary cover units is generally concealed by Quaternary deposits of the Danube valley (Fig. 1b, c), and only locally slivers of Jurassic and Cretaceous sediments are exposed as uplifted tilted blocks at the surface. Based on geological observations and drill hole data in the northern fault segment, the minimum vertical displacement is assumed to be between 900 and 1800 m (Andritzky et al. 1968) whereas the magnitude of horizontal slip is largely unknown.

Close to its northwestern termination, the Danube Fault is well exposed in the Donaustauf segment (Fig. 1). The basement escarpment that faces the Danube valley in this part of the fault zone (Scheuchenberg block, see also vertical areal view, Fig. 1c) consists of highly tectonized granite (cataclasites) with only few relics of primary igneous minerals (Fig. 2). Fracturing and intensive cataclasis is manifested in a 20–50 m broad zone. This zone passes laterally into less intensively deformed regions (100–200 m in width) and finally into nearly intact granite. Splays of the fault, marked by breccias, trend in N and NNW direction from the master fault (Fig. 1b). The undeformed granite is a biotite-granite with porphyric K-feldspar, known as “Kristallgranit” (Propach 1989) and it is cut by a small graben structure (the Donaustauf basin),

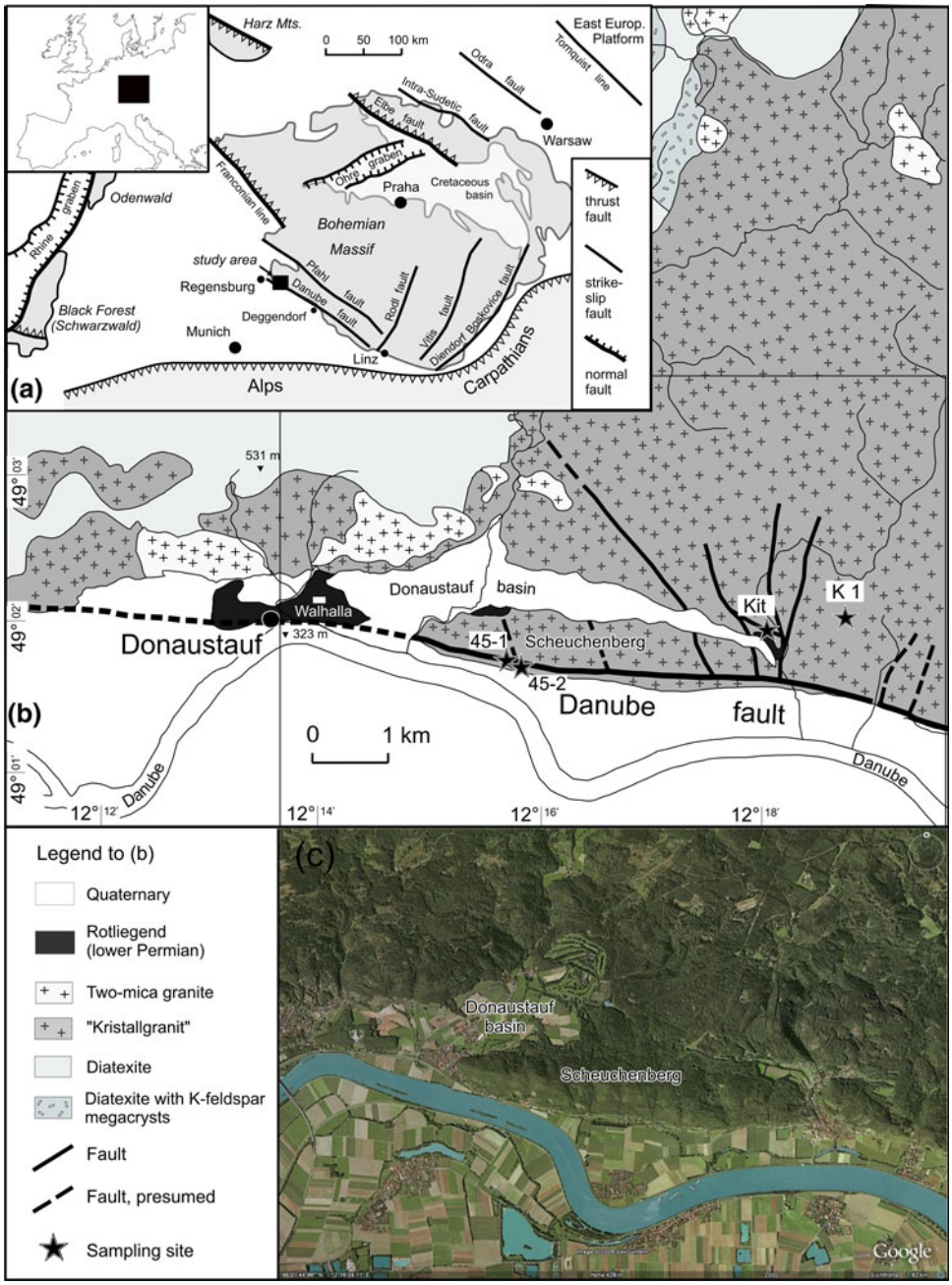

Fig. 1 **a** Geological map showing outline of Variscan basement outcrops in the foreland of the Alps and the location of major faults and lineament structures in central Europe (modified after Zulauf and Duyster 1997). The Bohemian Massif is dissected by a system of NW trending faults (including the Danube Fault) and conjugate structures running parallel to the Alpine-Carpathian orogenic front. **b** Geological map of the study area depicting the location of the Danube Fault, subsidiary splays of the fault associated with fluorite mineralization, distribution of the "Kristallgranit" and the narrow Permian graben structure (Donaustauf basin). Older graben fill sediments are concealed by Neogene and Quaternary deposits. Zones of strong cataclastic deformation are developed along the Danube Fault. Locations are shown where zircon Pb-evaporation and apatite fission track ages from undeformed granite (K1), K–Ar ages from cataclasites (45-1, 45-2) and (U–Th)/He dates from fluorite mineralization (Kit) have been obtained. **c** Google map satellite view depicting morphological features from the fault zone area (shown section framed in **b**)

which runs parallel to the Danube Fault (Fig. 1b, c). The graben is characterized by remnants of terrestrial Rotliegend sediments (Lower Permian; e.g. Mattern 1995).

Movement along the Danube Fault zone created brecciation zones and dilatant spaces within the Variscan basement rocks. Such zones, which are characterized by enhanced permeability, provided conduits for ascending hydrothermal solutions. In the study area, they were filled with veinlets, dikes and bands of purple and green fluorite, quartz and other vein minerals (Kraus 1958), and this gave rise to fluorite mining operations throughout the last centuries. Hydrothermal activity and alteration was accompanied by an argillization process during which most of the primary framework silicates were replaced by clay minerals.

Samples and analytical procedures

Four samples from three adjacent sites (Fig. 1b) were selected for geochronological and thermochronological investigation. Largely undeformed "Kristallgranit" (K1) was sampled from a small in situ bedrock outcrop located c. 1 km north of the main cataclastic zone (49°01′36″N,

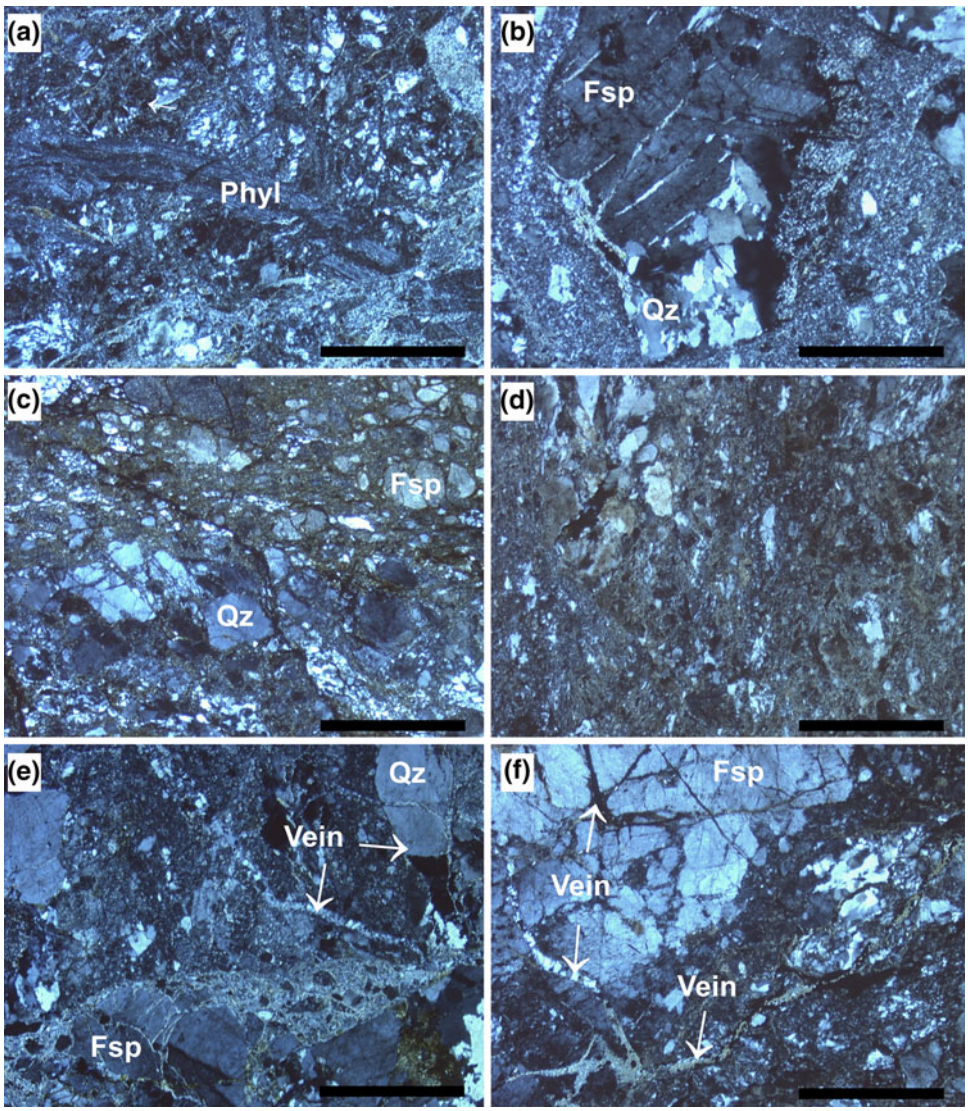

Fig. 2 Thin section photomicrographs under crossed polars giving an overview of cataclastic rocks from the Danube Fault, Donaustauf sector. The rocks are generally non-foliated or display poor schistosity. **a** Cataclasite with elongated cluster of phyllosilicates. **b** Relics of altered quartz–feldspar clast with intragranular fractures filled by fine grained mica (sericite) embedded in a clayey matrix. **c** Mesocataclasite with angular and subrounded clasts of feldspar and quartz and **d** Ultracataclasite with matrix occupying a greater total volume as in (**c**). **e–f** Cataclasites with numerous 0.1–0.5 mm wide veins filled with clay and quartz demonstrating that channelized fluids infiltrated the rock during and after cataclastic deformation. In (**f**), a quartz vein (left-hand side) infiltrates a pre-existing fracture of a feldspar clast whereas other fractures within this mineral (figure top) are filled by clay minerals. Width of scale bar in each subfigure is 1 mm. *Fsp* Feldspar, *Qz* quartz, *Phyl* phyllosilicate

12°19′06″E). Two cataclasites (sample 45-1, 49°01′28″N, 12°15′05″E and sample 45-2, 49°01′25″N, 12°15′25″E) were collected from abandoned quarries located in the centre of the main fault zone (Fig. 1b). Slumping made it impossible to approach the steep quarry walls and the samples had to be taken from rock slide material. Microscopy revealed pervasive cataclastic deformation without preferred fabric orientation (Fig. 2). Phyllosilicates formed during syntectonic alteration of feldspar, and with increasing clay content, the rocks acquired a progressively softer matrix. Intragranular fractured feldspar and the clay-rich matrix attests to a low temperature regime during cataclastic deformation, largely precluding plastic deformation of quartz. Healing of fractures by precipitation of late quartz veins is attributed to circulation of a late-stage fluid phase (Fig. 2). Another sample (Kit) comes from the vein-type Kittenrain fluorite deposit. This deposit lies within the Donaustauf (or Sulzbach) fluorite mining province (Fig. 1). The investigated fluorite specimen (Fig. 3), donated by the Bavarian Environment Agency, was collected from a mined vein located in a northwest-trending subsidiary fault splay (49°01′46″N, 12°18′02″E).

Zircon and apatite crystals were separated from the unaffected granite using conventional magnetic and heavy liquid techniques. For clay separation, the two cataclasite samples were reduced to chips and disaggregated by repetitive cycles of freeze and thaw to avoid artificial reduction of larger framework minerals (Liewig et al. 1987). After sieving (<63 μm), clay-size fractions (<2 μm) were obtained by differential settling in Atterberg cylinders. The mineral composition of the clay-size fractions was determined by X-ray diffraction (XRD) in untreated and glycol-treated states. SIROQUANT evaluation was performed twice on each sample and geochemical information was obtained by X-ray fluorescence (XRF).

Fig. 3 Alternating bands of purple and green fluorite from the Kittenrain mine, Donaustauf (or Sulzbach) fluorite mining district. Aliquots for fluorite (U–Th)/He dating were taken from this sample (Kit)

Zircon Pb-evaporation analyses (Kober 1987) were carried out at University of Tübingen using procedures described in Siebel et al. (2003).

K–Ar analyses on two clay-size fractions were carried out at the University of Göttingen. Potassium was determined in duplicate by flame photometry using an Eppendorf Elex 63/61.

Argon isotopic composition was measured in a pyrex glass extraction and purification line coupled to a VG 1200 C noble gas mass spectrometer operating in static mode.

For *Rb–Sr analyses* the illitic clay separates were leached for 10 min in 1 N HCl at room temperature prior to dissolution and separation by cation exchange chromatography. Analytical procedures for Rb-Sr separation are described in Siebel et al. (2005a, b). All isotopic measurements were made by Thermal Ionization Mass Spectrometry, on a Finnigan MAT 262 mass spectrometer at Tübingen University. Analyses of 12 separate loads of the NBS 987 Sr standard, during the course of this study yielded a mean $^{87}Sr/^{86}Sr$ ratio of 0.710254 ± 0.000014 (reference value = 0.710248).

Apatite fission track analysis was carried out in the Thermochronological Laboratory at University of Tübingen using standard procedures described by Danišík et al. (2007). We used the external detector method (Gleadow 1981) with the etching protocol of Donelick et al. (1999) and the zeta calibration approach to determine the age (Hurford and Green 1982). Low-temperature thermal history based on apatite fission track data (age and track length data) was modelled using the HeFTy program (Ketcham 2005).

For *(U–Th)/He analyses* fluorite shards were degassed under vacuum using laser-heating and analysed for He using a Pfeiffer Prisma QMS-200 mass spectrometer in the Thermochronological Laboratory at University of Tübingen. Following He measurements, the shards were analysed by isotope dilution for U and Th at the John de Laeter Centre of Mass Spectrometry in Perth (Australia) on an Agilent 7500 mass spectrometer. For more details on analytical procedures, reader is referred to Danišík (2005) and Evans et al. (2005). Final (U–Th)/He dates were not corrected for alpha recoil as the shards of fluorite were subsampled from the interior of a large crystal ~3 cm in diameter.

Results

Results of Pb-evaporation analyses of the "Kristallgranit" sample are shown in Fig. 4. The zircon grains are idiomorphic and inclusion-free. Cathodoluminescence images lack evidence of pre-magmatic or inherited zircon components (Fig. 4). Seven grains gave $^{207}Pb/^{206}Pb$ ages between 332.7 ± 3.3 and 314.4 ± 4.1 Ma. The average age is 324.6 ± 6.9 Ma (all age errors refer to the 95% confidence level, 2σ).

An apparent apatite fission track age of 217 ± 18 Ma was measured on the same sample (Table 1). The track length distribution (Fig. 5) was unimodal, positively skewed and relatively narrow (standard deviation: 1.4 μm). The mean track length was short (12.4 μm), which is typical of rocks with repetitive stay within, or slow cooling through the apatite partial annealing zone (~60–120°C; e.g. Gleadow et al. 1986a, b; Wagner and Van den haute 1992).

K–Ar analyses (Table 2) on the <2 μm clay-size fractions from two cataclasite samples yield ages of 266.1 ± 3.0 and 255.4 ± 3.2 Ma. The age discrepancy might be due to slight differences in the particle size range within the two samples rather than the presence of different amounts of relict (i.e. inherited from the host rock) mineral phases (see discussion below). The K_2O concentration (determined by flame-photometry) in both samples was high (~7.3%) as was the amount of radiogenic ^{40}Ar (>98%) indicating negligible atmospheric contamination.

The two illite fractions have slightly different Rb–Sr isotopic compositions (Table 2). When plotted on a graph of $^{87}Sr/^{86}Sr$ versus $^{87}Rb/^{86}Sr$ a two point isochron age of 258 ± 6 Ma is obtained (Fig. 6). The isochron shows an initial $^{87}Sr/^{86}Sr$ isotope ratio of 0.7212 ± 0.0035.

Chemical analyses (XRF data) of the two <2 μm fractions give virtually the same composition: 52.5% SiO_2, 23.7% Al_2O_3, 7.3% K_2O, 6.1% Fe_2O_3, 2.4% MgO and 5.7% loss of ignition (the latter is mainly a measure of H_2O content); other major elements are below 1%.

Special attention was paid to ensure that illite was the major clay mineral in the dated samples and that no relict

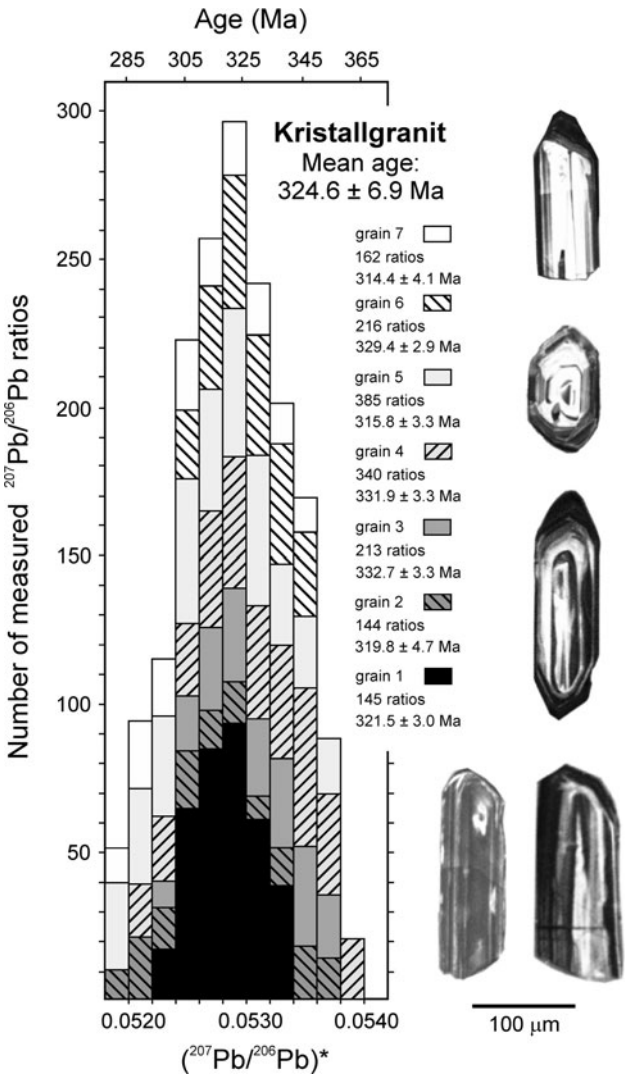

Fig. 4 Frequency histogram showing the distribution of radiogenic (*) $^{207}Pb/^{206}Pb$ ratios obtained from Pb-evaporation of seven different zircon crystals from the "Kristallgranit" sample K1. Age information and number of measured $^{207}Pb/^{206}Pb$ ratios for individual grains (labelled 1–7) is given at the right hand side of the diagram. Photographs show cathodoluminescence images of zircon crystals similar, but not identical to those analysed for age determination. For sample location see Fig. 1b and text

phases (e.g. feldspar, mica) that would result in inconclusive older ages were present. XRD results show that the two dated clay-size fractions consisted mostly of illite with only minor amounts of kaolinite and traces of quartz. The XRD diagram for the glycol-treated runs showed no shift of peaks or change in peak shapes. This lack of mixed-layer reflections points to the absence of interstratified illite-smectite or kaolinite-smectite species. The lack of change of a weak 14 Å peak is indicative of the (001) reflex of chlorite. No detectable primary minerals (feldspar, biotite) could be identified and the compositions derived from SIROQUANT analysis are:

$$\text{Sample } 45-1: \sim 82\%\ \text{illite},\ \sim 10\%\ \text{kaolinite},\ \sim 3\%\ \text{chlorite},\ \sim 5\%\ \text{quartz}$$

$$\text{Sample } 45-4: \sim 86\%\ \text{illite},\ \sim 7\%\ \text{kaolinite},\ \sim 1\%\ \text{chlorite},\ \sim 6\%\text{quartz}$$

The fluorite (U–Th)/He dating results are shown in Table 3. The two investigated shards yield ages of 127 ± 18 and 110 ± 15 Ma.

Discussion

Initiation of the Danube Fault

The "Kristallgranit" has been the site of faulting within the Donaustauf segment of the Danube Fault. Its emplacement at 325 ± 7 Ma as determined by the zircon evaporation method occurred during a time of major magma production in the region (Siebel et al. 2008). Despite some age scatter which might reflect a weak influence of the shear zone upon the U–Pb zircon system (Fig. 4), a strong isotopic disturbance resulting from fault activity seems unlikely since the rock was sampled at c. 1 km distance from the fault zone (Fig. 1b). Based on whole-rock analyses from 11 sampling sites, Köhler and Müller-Sohnius (1986) obtained a Rb–Sr isochron age of 349 ± 11 Ma for the

Table 1 Apatite fission track results on a sample from "Kristallgranit"

Sample	N	ρ_s	N_s	ρ_i	N_i	ρ_d	N_d	$P(\chi^2)$ %	Age (Ma)	$\pm 2\sigma$ (Ma)	MTL (µm)	SD (µm)	SE (µm)	N(L)	Dpar (µm)
K1	20	77.06	2355	37.598	1149	7.055	2801	92	218	18	12.4	1.4	0.1	111	1.65

N Number of dated apatite crystals, ρ_s (ρ_i) spontaneous (induced) track densities ($\times 10^5$ tracks/cm^2), N_s (N_i) number of counted spontaneous (induced) tracks, ρ_d dosimeter track density ($\times 10^5$ tracks/cm^2), N_d number of tracks counted on dosimeter, $P(\chi^2)$ probability obtaining Chi-square value for n degree of freedom (where n = no. of crystals − 1), Age ± 1σ central age ± 1 standard error (Galbraith and Laslett 1993), *MTL* mean track length, *SE* standard error of mean track length, *SD* standard deviation of track length distribution, *N*(L) number of horizontal confined tracks measured, *Dpar* average etch pit diameter of fission tracks

Age was calculated using zeta calibration method (Hurford and Green 1982), glass dosimeter CN-5, and zeta value of 305.98 ± 4.25 year/cm^2

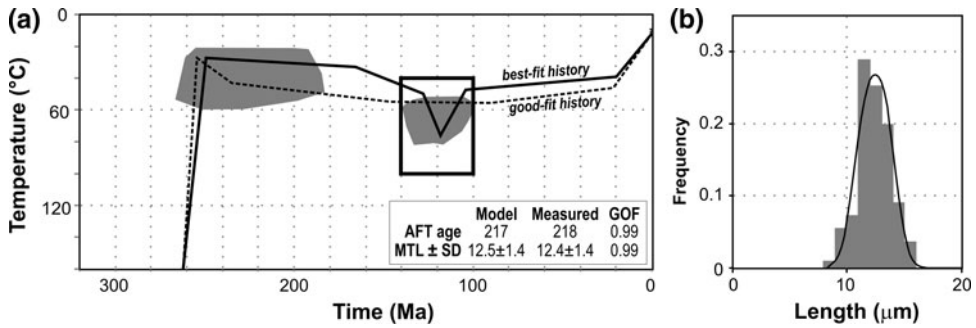

Fig. 5 **a** Thermal modelling results of AFT data of the "Kristallgranit" sample K1 obtained with HeFTy modelling program (Ketcham 2005) using the multikinetic annealing model of Ketcham et al. (1999). The best-fit history is shown as a *solid black line*; *shaded polygons* show the ranges of acceptable values of minimum/maximum temperatures; *black box* is the constraint set according to blocking temperature of fluorite and measured (U–Th)/He ages. *Dashed line* ('good-fit history') indicates a solution, which reconciles the measured data, but does not require a thermal event in the Cretaceous (see "Discussion" section for further explanation). MTL is mean track length in μm; SD is standard deviation in μm; GOF is goodness of fit (statistical comparison of the measured input data and modelled output data, where a "good" result corresponds to value 0.5 or higher, "the best" result corresponds to value 1). **b** Frequency distribution of measured confined track length data overlain by a calculated probability density function (best fit)

Table 2 Results of K–Ar and Rb–Sr analyses of two <2 μm clay-size fractions from the Danube Fault

Sample	Size (μm)	K_2O (%)	Radiogenic Ar		K–Ar age (Ma ± 2σ)	Rb (ppm)	Sr (ppm)	$^{87}Rb/^{86}Sr$	$^{87}Sr/^{86}Sr$
			(nl/g) STP	(%)					
45-1	<2	7.28	64.41	99.04	255.4 ± 3.2	578.5	47.4	35.83	0.852722
45-2	<2	7.34	67.86	98.66	266.1 ± 3.0	641.4	34.1	55.49	0.924894

STP Standard temperature and pressure

Analytical error for K/Ar age is given on a 95% confidence level (2σ)

"Kristallgranit". Propach et al. (2000) reported concordant U–Pb zircon ages of 315 ± 4 Ma and two concordant monazite ages of 317 ± 3 and 318 ± 3 Ma of another "Kristallgranit" sample sampled c. 8 km north of the fault zone (49°05′06″N, 12°23′10″E).

The "Kristallgranit" is interpreted as a lower crustal anatectic melt, most of which did not migrate far from the source region (see also Propach 1989). Evidence for this is noted at several localities where gradual transitions into migmatite structures occur. Although no direct barometric data is available from the "Kristallgranit", these outcrop relationships, as well as pressure estimates from adjacent basement rocks and granites (Kalt et al. 2000; Klein et al. 2008) suggest that magma emplacement occurred at depths greater than 10–15 km.

The "Kristallgranit" has no preferred outcrop shape or alignment parallel with the fault as would be expected if the Danube Fault was active during the time of granite emplacement. In addition, at lower crustal levels, fault-related synmagmatic deformation should have caused ductile deformation of the "Kristallgranit" which is not observed. From these arguments we infer that the Donaustauf segment of the Danube Fault started to form after the intrusion of the "Kristallgranit", i.e. when the granite was uplifted from depth to brittle levels of the crust.

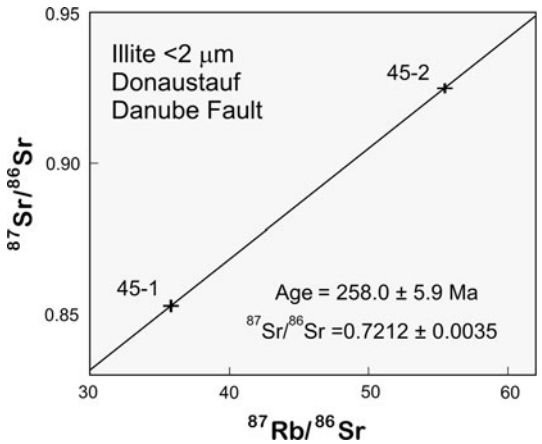

Fig. 6 Two point Rb–Sr isochron plot for illitic clay fractions of samples 45-1 and 45-2

For the adjacent Bavarian Pfahl fault zone it was argued that the initiation of fracturing was ultimately linked to the emplacement of granodioritic augengneisses parallel to this fracture zone at c. 330–335 Ma (Siebel et al. 2005a, b). Thus, it can be inferred that the movements along the Danube Fault post-date the initiation of the Bavarian Pfahl shear zone by at least 10 Ma.

Table 3 Results of (U–Th)/He dating of the fluorite from the Kittenrain mine, Danube Fault

Sample	N_s	Th (ng)	Th error (%)	U (ng)	U error (%)	^{4}He (ncc at STP)	^{4}He error (%)	TAU (%)	Th/U	F_t	Age (Ma ± 2σ)
Kit#1	1	0.0083	4.9	0.0041	4.8	0.082	0.9	5.0	2.01	1	110.2 ± 15
Kit#2	1	0.0062	5.3	0.0044	4.8	0.092	0.9	5.2	1.40	1	127.4 ± 18

N_s Number of fluorite shards analysed, *TAU* total analytical uncertainty, F_t alpha recoil correction factor (Farley et al. 1996)

It has been suggested that the Danube Fault started to form under greenschist facies conditions at temperatures of c. 450°C (Brandmayr et al. 1995; Mattern 1995), i.e. above the brittle–ductile transition zone in quartz–feldspar bearing rocks. Based on observations at the Deggendorf fault segment, 60 km further southeast of our study area, Schreyer (1967) argued that the Danube Fault had been formed as a late-Variscan ductile shear zone. The time of ductile deformation was constrained by a ^{40}Ar/^{39}Ar muscovite age from the Austrian section of the fault at 287.3 ± 0.6 Ma (on mylonitic paragneiss, Platzer 1992; Brandmayr et al. 1995). Muscovites from the syn-kinematically deformed Haibach granite sample outside the shear zone define a ^{40}Ar/^{39}Ar plateau age of 288.5 ± 0.6 Ma. A similar white-mica age (281.3 ± 0.6 Ma) was reported for the NE–SW trending Rödl shear zone, Austria (Brandmayr et al. 1995).

In the Austrian section of the Danube Fault several mesoscopic ductile shear fabrics (e.g. mylonitic foliations, synkinematic recrystallization of quartz) are well preserved (Brandmayr et al. 1995), whereas along the Donaustauf fault sector a brittle deformation regime is evidently indicated by the occurrence of cataclastic rocks. It is possible that different structural levels along the fault are exposed today and that the Donaustauf segment represents a shallower fault zone level. Alternatively, the Donaustauf sector of the shear zone started to form at higher temperatures but experienced a much stronger brittle overprint relative to the Austrian part. The fact that at the Donaustauf fault segment brittle deformation structures are prevalent enables us to constrain the brittle deformation stage of the fault as discussed in the next section.

Cataclastic deformation and reactivation of the Danube Fault

The illite fractions yield Late Permian K–Ar and Rb–Sr ages. Under static conditions illite crystals between 0, 1 and 2 μm in size (i.e. in the range of the material which was analysed) retain argon at temperatures between 200 and 250°C (see Hunziker et al. 1986; Hames and Bowring 1994; Hodges 2003). The illite ages imply that temperatures above this range did not prevail in the fault zone after 255 Ma.

The illites were extracted from central fault zone samples in which the original minerals were almost completely altered into clay-rich material (Fig. 2). In granite, illite can form as a hydrothermal alteration product of feldspar or white mica. Since the protolith ("Kristallgranit") contained no primary muscovite (see also Propach 1989), most of the illite must have been produced by decomposition of K-feldspar under static hydrous conditions basically following the reaction:

$$3KAlSi_3O_8 + 2H^+ + 12H_2O \rightarrow KAl_3Si_3O_{10}(OH)_2 + 2K^+ + 6H_4SiO_4.$$

The geochemical composition (XRF data) determined for the two clay-size fractions (i.e. 52.5% SiO_2, 23.7% Al_2O_3, 7.3% K_2O, 6.1% Fe_2O_3, 2.4% MgO) is virtually identical to the chemical composition reported for pure illite (e.g. Su and Suarez 2004). Some of the magnesium and iron was probably acquired by the illites from degrading biotite, or (to a lesser extent) can be attributed to the presence of chlorite in the sample. Since illite is the dominant clay mineral in the <2 μm fractions and kaolinite, chlorite and quartz contain very little potassium and rubidium, the K–Ar and Rb–Sr ages are thus determined by the illite crystals.

The Donaustauf basin, which cuts the "Kristallgranit", received detrital (Rotliegend) sediments (derived from the graben shoulders; Fig 1b) in the Early Permian. This provides geological evidence for uplift and erosion of the Variscan basement and tectonic extension at a time period prior to that bracketed by the K–Ar and Rb–Sr illite ages (i.e. 266–255 Ma). Final exhumation of the basement is recorded by the thermal modelling results based on the apatite fission track data of the "Kristallgranit" sample, which suggest that the sample reached near-surface temperature conditions during Permo-Triassic times (see Fig. 5 and explanation below). From these observations we conclude that the illite crystals were formed at temperatures sufficiently below their Ar blocking interval (i.e. <200–250°C) and consequently, do not date a cooling event. The ages are more likely to date the formation of the minerals.

The Bavarian Pfahl fault (Fig. 1a) localizes a huge quartz dike. This dike as well as similar quartz filled extensional veins east of Donaustauf (Hann et al. 2007) was formed by tectonically driven epithermal fluid infiltration events (Peucker-Ehrenbrink and Behr 1993). The quartz mineralization age of 247 ± 21 Ma (Horn et al. 1986) is close to our illite ages from the Danube Fault.

Since there was significant hydrothermal activity during the Permo-Triassic (further evidence for this given below), the illites along the Donaustauf sector of the Danube Fault could have developed during a hydrothermal alteration and vein-filling event at the end of the cataclastic deformation phase.

The (U–Th)/He fluorite dates from the Kittenrain fluorites failed to deliver tight age constraints for the mineralization event. Kraus (1958) argued that the fluorite precipitated from meso- and epithermal solutions at temperatures between c. 300–100°C. Based on the illite ages, such high-temperature fluids are unlikely to have existed during the Mesozoic but were more likely connected with fluids originating from late-Variscan heat sources. The hydrothermal mineralization in the Nabburg-Wölsendorf fluorite mining province, 50 km north of the Donaustauf area, was dated as Permian (K–Ar and Rb–Sr ages of authigenic K-feldspar of 254 ± 6 Ma, Brockamp and Zuther 1985 and 264 ± 4 Ma, Lippolt et al. 1985, respectively), i.e. coeval with the illite formation in our study area. U–Pb-dating of pitchblende from the same mining province gave somewhat older ages (295 ± 14 Ma, Carl and Dill 1984). From these ages it can be concluded that the fluorite formation was a Permian process and that the helium in the Kittenrain fluorites was not fully retained during subsequent geological processes.

The blocking temperature of helium in fluorite is between 100 and 55°C, the exact value depending on cooling rate (Evans et al. 2005; Pi et al. 2005). The obtained ages depend on the complexity of the low-temperature cooling history and of particular importance is how long the mineral resided in the helium partial retention zone (Wolf et al. 1998). The (U–Th)/He dates can (i) be related to some geological event in the Early Cretaceous, or (ii) result from slow cooling through the partial retention zone. In the latter case the measured age would not be related to any specific geological event. During the Jurassic and Late Cretaceous (Cenoman-Turon), marine sediments sealed the Danube Fault mainly to the northwest and southwest of its present-day exposure. In contrast, the block northeast of the Danube Fault was an uplifted area only sporadically covered by the sea. In this context, it is also important to consider the potential effect of Mesozoic or Alpine reactivation of the Danube Fault (e.g. Thiele 1961). Mesozoic reactivation was reported for other lineaments at the margin of the Bohemian Massif, e.g. the Franconian Line (Zulauf and Duyster 1997). Evidence for reactivation of the Danube Fault zone with a dip-slip component comes from the vertical displacement of the Mesozoic (Jurassic/Cretaceous) sediments (Andritzky et al. 1968). Fracturing of the rocks and frictional heating during this event may have caused helium loss in the fluorites (comp. Evans et al. 2005; Pi et al. 2005).

In order to test this possibility and quantify the magnitude of Early Cretaceous thermal overprint during fault reactivation, we modelled time–temperature trajectories of the "Kristallgranit" sample (Fig. 5a). Fluorite (U–Th)/He ages were converted into time–temperature data in the form of a box set at $T = 40$–100°C and 140–100 Ma (according to blocking temperature and (U–Th)/He ages, respectively). The modelling results validate the hypothesis of thermal overprint between ~140 and ~100 Ma with maximum temperatures between 50 and 80°C (Fig. 5). This temperature range is high enough to fully reset the fluorite (U–Th)/He thermochronometer, but too low to fully reset the apatite fission track system. However, it has to be kept in mind that this is a specific solution for the data and in fact, a scenario with thermal stagnation during the whole Mesozoic and Cenozoic with no thermal event in the Cretaceous cannot be completely ruled out by the thermal modelling results (see dashed line (good-fit history) solution in Fig. 5).

Summary of fault chronology

Major shear zones in the Bohemian Massif have been initiated during late-Palaeozoic strike slip faulting of the Variscan basement (Mattern 1995, 2001). The Danube Fault zone, which cuts granite, underwent ductile and brittle deformation followed by hydrous argillic alteration. When the geochronological results of this study are compared with previously published age data from this and other shear zones and hydrothermal mineral deposits in the western Bohemian Massif, the following fault zone chronology can be established: The emplacement age of the original rock, "Kristallgranit" (325 ± 7 Ma) gives an upper age limit for shear zone activity. Based on this data it can be inferred that the Danube fault became active c. 10 Ma later than the Bavarian Pfahl zone (Siebel et al. 2005a, b). White micas post-date high temperature ductile deformation of rocks within the Austrian sector of the Danube Fault (~375 ± 25°C) around 280–290 Ma (Brandmayr et al. 1995). The new K–Ar (266 ± 4, 255 ± 3 Ma) and Rb–Sr (258 ± 6 Ma) illite dates of this study are interpreted to constrain the end of cataclastic deformation in the Donaustauf sector of the fault. In this sector, breccia zones along splays of the master fault were mineralized by hydrothermal fluorite. Infiltration of cataclastic zones by fluids and precipitation of hydrothermal mineral deposits occurred between 264 and 254 Ma (Nabburg-Wölsendorf mining province, Brockamp and Zuther 1985, Lippolt et al. 1985) and around 247 ± 21 Ma (Pfahl quartz lode, Horn et al. 1986). As evidenced by apatite fission track data, the rocks of the investigated fault segment were already experiencing paleo-temperatures below 60°C during the Triassic. A later reactivation of the

Danube Fault during the Cretaceous is indicated by the vertical offset of Mesozoic strata and the reset of the (U–Th)/He fluorite system.

Conclusions

The use of multi-method geochronology can place time constraints on initiation, brittle growth and reactivation (reheating) of ancient basement faults. This approach can be extended to other reactivated fault localities providing the presence of both primary magmatic and secondary mineral phases and the employment of high-and low-temperature isotopic chronometers. The distinction between cooling following erosion-driven rock uplift and cooling following fault reactivation by frictional heating, however, remains difficult without additional geological constraints.

Acknowledgments Field research and mapping in the Donaustauf area was sponsored by the Bayerisches Landesamt für Umwelt, LfU. We especially appreciate the efforts of Dr. Schwarzmeier in this respect. Special thanks are extended to Sandra Gorse and Miriam Ringwald for the separation and characterization of the illite fine-fractions. The paper benefited from stimulating suggestions of W. Frisch. Our thanks go to W.-C. Dullo, J. Imber, K. Mezger, U. Schaltegger, G. Zulauf and an anonymous reviewer for critical and constructive comments which helped to clarify our presentation and to improve older versions of the manuscript.

References

Andritzky G, Bauberger W, Hergert G, Köhler H, Schricke W, Tillmann H, Troll G (1968) Führer zu geologisch-petrographischen Exkursionen im Bayerischen Wald. Teil II: Aufschlüsse im Westteil: Regensburger Wald. Geol Bavarica 59: 1–88

Banerjee D, Singhvi AK, Pande K, Gogte VD, Chandra BP (1999) Towards a direct dating of fault gouges using luminescence dating techniques—methodological aspects. Curr Sci 77:256–268

Brandmayr M, Dallmeyer RD, Handler R, Wallbrecher E (1995) Conjugate shear zones in the Southern Bohemian Massif (Austria): implications for Variscan and Alpine tectonothermal activity. Tectonophysics 248:97–116

Brockamp O, Zuther M (1985) K/Ar-Datierungen zur Alterseinstufung lagerstättenbildender Prozesse. Naturwissenschaften 72:141–143

Carl C, Dill H (1984) U/Pb Datierung an Pechblende aus dem Nabburg-Wölsendorfer Flußspatrevier. Geol Jahrb D63:59–76

Danišík M (2005) Cooling history and relief evolution of Corsica (France) as constrained by fission track and (U-Th)/He thermochronology. Tübinger Geowiss Arb A72:130 pp

Danišík M, Kuhlemann J, Dunkl I, Székely B, Frisch W (2007) Burial and exhumation of Corsica (France) in the light of fission track data. Tectonics 26:TC1001. doi:10.1029/2005TC001938

Donelick RA, Ketcham RA, Carlson WD (1999) Variability of apatite fission-track annealing kinetics: I. Experimental results. Am Mineral 84:1224–1234

Evans NJ, Wilson NSF, Cline JS, McInnes BIA, Byrne J (2005) Fluorite (U-Th)/He thermochronology: constraints on the low temperature history of Yucca Mountains, Nevada. Appl Geochem 20:1099–1105

Eyal Y, Kaufman A, Bar-Matthews B (1992) Use of ^{230}Th/U ages of striated carnotites for dating fault displacements. Geology 20:829–832

Farley KA, Wolf RA, Silver LT (1996) The effect of long alpha-stopping distances on (U-Th)/He ages. Geochim Cosmochim Acta 60:4223–4229

Fenton CR, Webb RH, Pearthree PA, Cerling TE, Poreda RJ (2001) Displacement rates on the Toroweap and Hurricane faults: implications for quaternary downcutting in the Grand Canyon, Arizona. Geology 29:1035–1038

Galbraith RF, Laslett GM (1993) Statistical models for mixed fission track ages. Nucl Tracks Radiat Meas 21:459–470

Gleadow AJW (1981) Fission-track dating methods: what are the real alternatives? Nucl Tracks Radiat Meas 5:3–14

Gleadow AJW, Duddy IR, Green PF (1986a) Fission track lengths in the apatite annealing zone and the interpretation of mixed ages. Earth Planet Sci Lett 78:245–254

Gleadow AJW, Duddy IR, Green PF (1986b) Confined fission track lengths in apatite: a diagnostic tool for thermal history analysis. Contrib Mineral Petrol 94:405–415

Hames P, Bowring SA (1994) An empirical evaluation of the argon diffusion geometry in muscovite. Earth Planet Sci Lett 124:161–167

Hann HP, Rohrmüller H, Siebel W (2007) Quartz-filled extensional veins in the basement of Vorderer Bayerischer Wald. N Jahrb Geol Paläont Abh 244:197–205 (in German with English abstract)

Hodges KV (2003) Geochronology and thermochronology in orogenic systems. In: Rudnick RL (ed) The crust. Treatise on Geochemistry 3. Elsevier-Pergamon, Oxford, pp 263–292

Horn P, Köhler H, Müller-Sohnius D (1986) The Rb–Sr isotope geochemistry of hydrothermal quartz from the Bayerischer Pfahl and a fluorite-barite vein from Nabburg-Wölsendorf, Federal Republic of Germany. Chem Geol 58:259–272 (in German with English abstract)

Hunziker JC, Frey M, Clauer N, Dallmeyer RD, Friedrichsen H, Flehmig W, Hochstrasser K, Roggwiler P, Schwander H (1986) The evolution of illite to muscovite: mineralogical and isotopic data from the Glarus Alps, Switzerland. Contrib Mineral Petrol 92:157–180

Hurford AJ, Green PF (1982) A user's guide to fission-track dating calibration. Earth Planet Sci Lett 59:343–354

Ikeya M, Miki T, Tanaka K (1982) Dating of a fault by electron spin resonance on intrafault materials. Science 215:1392–1393

Kalt A, Corfu F, Wijbrans JR (2000) Time calibration of a P-T path from a Variscan high-temperature low-pressure metamorphic complex (Bayerische Wald, Germany), and the detection of inherited monazite. Contrib Mineral Petrol 138:143–163

Ketcham RA (2005) Forward and inverse modeling of low-temperature thermochronometry data. In: Reiners PW, Ehlers TA (eds) Low-temperature thermochronology: techniques, interpretations, and applications. Rev Mineral Geochem 58:275–314

Ketcham RA, Donelick RA, Carlson WD (1999) Variability of apatite fission-track annealing kinetics: III. Extrapolation to geologic time scales. Am Mineral 84:1235–1255

Klein P, Kiehm S, Siebel W, Shang CK, Rohrmüller J, Dörr S, Zulauf G (2008) Age and emplacement of late-Variscan granites of the western Bohemian Massif with main focus on the Hauzenberg granitoids. Lithos 102:478–507

Kober B (1987) Single-zircon evaporation combined with Pb+ emitter-bedding for ^{207}Pb/^{206}Pb-age investigations using thermal ion mass spectrometry, and implications to zirconology. Contrib Mineral Petrol 96:63–71

Köhler H, Müller-Sohnius D (1986) Rb–Sr age determinations and Sr-isotope systematic of rocks from the Regensburger Wald

(Moldanubikum NE Bavaria)—part 2: intrusives. N Jahrb Miner Abh 155:219–241 (in German with English abstract)
Kohút M, Sherlock SC (2003) Laser microprobe $^{40}Ar/^{39}Ar$ analysis of pseudotachylite and host rocks from the Tatra Mountains, Slovakia: Late Paleocene seismicity and implications for sediment supply. Terra Nova 15:417–424
Kralik M, Klima K, Riedmjller G (1987) Dating fault gouges. Nature 327:315–317
Kraus G (1958) Tektonik und Genese der Flußspatgänge östlich von Regensburg, Bayerischer Wald. N Jarhb Miner Abh 92:109–146
Liewig N, Clauer N, Sommer F (1987) Rb-Sr and K-Ar dating of clay diagenesis in Jurassic sandstone oil reservoir, North Sea. Am Assoc Pet Geol Bull 71:1467–1474
Lippolt HJ, Mertz DF, Ziehr H (1985) The late Permian Rb-Sr age of K-feldspar from the Wölsendorf mineralisation (Oberpfalz, FR Germany). N Jahrb Miner Mh 1985:49–57
Lyons JB, Snellenburg J (1971) Dating faults. Geol Soc Am Bull 82:1749–1751
Mattern F (1995) Late Carboniferous to early Triassic shear sense reversals at strike-slip faults in eastern Bavaria. Zbl Geol Paläontol Teil I 1993:1471–1490
Mattern F (2001) Permo-Silesian movements between Baltica and western Europe: tectonics and 'basin families'. Terra Nova 13:368–375
Murakami M, Tagami T (2004) Dating pseudotachylyte of the Nojima fault using the zircon fission-track method. Geophys Res Lett 31:L12604
Parry WT, Bunds MP, Bruhn RL, Hall CM, Murphy JM (2001) Mineralogy, $^{40}Ar/^{39}Ar$ dating and apatite fission track dating of rocks along the Castle Mountain fault, Alaska. Tectonophysics 337:149–172
Peucker-Ehrenbrink B, Behr HJ (1993) Chemistry of hydrothermal quartz in the post-Variscan "Bavarian Pfahl" system, F.R. Germany. Chem Geol 103:85–102
Pi T, Solé J, Taran Y (2005) (U-Th)/He dating of fluorite: application of the La Azul fluorspar deposit in the Taxco mining district, Mexico. Mineral Deposita 39:976–982
Platzer R (1992) Kinematik und Alter der Donaustörung bei Schlögen (südliche Böhmische Masse, Oberösterreich). Frankf Geowiss Arb A11:141–144
Propach G (1989) The origin of a conformable Variscan granite in Bavaria—results of geochemical and geochronological investigations. In: Bonin B et al (eds) Geochemical and geophysical aspects of the interactions and evolution of magmas and rocks of the crust. Theophrastus Publications, Athens, pp 193–209
Propach G, Baumann A, Schulz-Schmalschläger M, Grauert B (2000) Zircon and monazite U-Pb ages of Variscan granitoid rocks and gneisses in the Moldanubian zone of eastern Bavaria, Germany. N Jahrb Geol Paläontol 2000:345–377
Ritz JF, Brown ET, Bourlès DL, Philip H, Schlupp A, Raisbeck GM, Yiou F (1995) Slip rates along active faults estimated with cosmic ray exposure dates: applications to the Bogd fault, Gobi-Altai, Mongolia. Geology 23:1019–1022
Schreyer W (1967) Das Grundgebirge in der Umgebung von Deggendorf an der Donau. Geol Bavarica 58:77–85
Sherlock SC, Watts LM, Holdsworth RE, Roberts D (2004) Dating fault reactivation by Ar/Ar laserprobe: an alternative view of apparently cogenetic mylonite-pseudotachylite assemblages. J Geol Soc London 161:335–338
Siebel W, Chen F, Satir M (2003) Late-Variscan magmatism revisited: new implications from Pb-evaporation zircon ages on the emplacement of redwitzites and granites in NE Bavaria. Int J Earth Sci (Geol Rundsch) 92:36–53
Siebel W, Blaha U, Chen F, Rohrmüller J (2005a) Geochronology and geochemistry of a dyke-host rock association and implications for the formation of the Bavarian Pfahl shear zone, Bohemian Massif. Int J Earth Sci (Geol Rundsch) 94:8–23
Siebel W, Reitter E, Wenzel T, Blaha U (2005b) Sr isotope systematics of K-feldspar in plutonic rocks revealed by the Rb-Sr microdrilling technique. Chem Geol 222:183–199
Siebel W, Shang CK, Reitter E, Rohrmüller H, Breiter K (2008) Two distinctive granite suites in the south-western Bohemian Massif and their record of emplacement: constraints from zircon $^{207}Pb/^{206}Pb$ chronology and geochemistry. J Petrol 49:1853–1872
Solum JG, van der Pluijm BA, Peacor DR (2005) Neocrystallization, fabrics and age of clay minerals from an exposure of the Moab Fault, Utah. J Struct Geol 27:1563–1576
Su C, Suarez DL (2004) Boron release from weathering of illites, serpentine, shales, and illitic/palygorskitic soils. Am J Soil Sci 68:96–105
Thiele O (1961) Zum Alter der Donaustörung. Verh Geol Bundesanst Österreich 1961:131–133
Wagner GA, Van den haute P (1992) Fission-track dating. Enke, Stuttgart, p 285
Wolf RA, Farley KA, Kass DM (1998) Modeling of the temperature sensitivity of the apatite (U-Th)/He thermochronometer. Chem Geol 148:105–114
Ylagan RF, Kim CS, Pevear DR, Vrolijk PJ (2002) Illite polytype quantification for accurate K-Ar age determination. Am Mineral 87:1536–1545
Zhao MW, Ahrendt H, Wemmer K (1997) K-Ar systematics of illite/smectite in argillaceous rocks from the Ordos basin, China. Chem Geol 136:153–169
Ziegler PA, Dézes P (2006) Crustal evolution of western and central Europe. Geol Soc Lond Mem 32:43–56
Zulauf G, Duyster J (1997) Supracrustal intraplate thickening of Variscan basement due to Alpine foreland compression: results from the superdeep well KTB (Bohemian Massif, Germany). Tectonics 16. doi:10.1029/97TC01656
Zwingmann H, Clauer N, Gaupp R (1999) Structure related geochemical (REE) and isotopic (K-Ar, Rb-Sr, $\delta^{18}O$) characteristics of clay minerals from Rotliegend sandstone reservoirs (Permian, northern Germany). Geochim Cosmochim Acta 63:2805–2823
Zwingmann H, Offler R, Wilson T, Cox SF (2004) K-Ar dating of fault gouge in the northern Sydney basin, NSW Australia—implications for the breakup of Gondwana. J Struct Geol 26:2285–2295